Targeted energy transfer from a resonant room to a hybrid electro-acoustic nonlinear membrane absorber: numerical and experimental study

Pierre-Yvon Bryk, Renaud Côte, Sergio Bellizzi

Targeted energy transfer from a resonant room to a hybrid electro-acoustic nonlinear membrane absorber: numerical and experimental study

Pierre-Yvon Bryk[a], Renaud Côte[a,*], Sergio Bellizzi[b]

[a] *Aix Marseille Univ, CNRS, Centrale Marseille, LMA, Marseille, France*
[b] *LMA, CNRS, UMR 7031, Centrale Marseille, Aix-Marseille Univ*

Abstract

We present the first real size evidence of targeted energy transfer in a concrete building, with an efficient action on low frequency noise reduction. It is achieved by the means of a hybrid Electro-Acoustic Nonlinear Energy Sink (EA-NES). The EA-NES action is based on targeted energy transfer. As in previous works the EA-NES is made of two elements: a membrane with a nonlinear dynamics, and an active system based on a loudspeaker which controls the pressure applied to the rear face of the membrane. We study here a proportional feedback control law driving the loudspeaker in current mode, and compare it with the voltage mode command law. The experiment is fully modeled. A singular perturbation method around a 1:1 resonance is used to find the slow critical manifold of the system and its dependence on the control loop gain for the two driving modes, in view of finding conditions allowing Strongly Modulated Regime (SMR). A good quantitative agreement is found between the model and the experiments. In the experimental study

*Corresponding author
Email address: cote@lma.cnrs-mrs.fr (Renaud Côte)

we observe a range in the excitation level corresponding to SMR where the sound level in the room is limited. We study the influence of its parameters on the thresholds of the working range of the EA-NES. We measure up to 8 dB of attenuation around 43 Hz.
Keywords: Nonlinear absorber, Targeted energy transfer, Periodic excitation, Acoustic resonance, Noise reduction

1. Introduction

It is always a challenge to reduce low-frequency noise transmission through an enclosure as for example in the case of acoustic enclosures for machine noise attenuation. Recent works focus on passive, active and hybrid active/passive devices. In [1, 2], the authors study passive acoustic resonators used as noise absorbers. In [3, 4], electro-acoustic absorbers are proposed. They are based on the use of an enclosed loudspeaker including an electric load that shunts the loudspeaker electrical terminals. An electro-acoustic absorber can either be passive or active in terms of external power, including pressure or velocity feedback techniques. In [5, 6], loudspeakers have also been used to design an active system which controls the normal impedance of surfaces in a room. Two approaches have been developed. The first is referred to as direct control: the acoustic pressure is measured close to the diaphragm of the loudspeaker and used to produce the desired impedance. In the second approach, passive and active means are combined: the rear face of a porous layer is actively controlled so as to make the front face normal impedance take a prescribed value. In [7], devices involving loudspeakers for active/passive control of both absorption and transmission are investigated.

This challenge is considered here through the relatively new concept of Targeted Energy Transfer (TET). TET is based on a coupling between a primary system (which vibrations must be mitigated) and a nonlinear absorber. The principle is to place the coupled system on one of its nonlinear modes in order to produce quasi-irreversible transfers of the vibratory energy from the primary system to the nonlinear absorber. This phenomenon is called energy pumping [8] and the nonlinear absorber is known as NES for Nonlinear Energy Sink. A basic NES generally consists of a light mass, an essentially nonlinear spring and a viscous linear damper. In the field of structural vibration, a wide variety of NES designs has been proposed, with different types of stiffness (cubic , non-polynomial, non-smooth nonlinearities...) [9, 10, 11, 12].

In acoustics, two types of NES have been proposed, one named acoustic NES based on an Helmholtz resonator with nonlinear behaviors [13], the other named vibroacoustic NES based on the use of a simple thin clamped structure involving geometric nonlinearity at large displacement. In [14, 15, 16], the thin clamped structure consists of a simple thin circular latex (viscoelastic) membrane whereas in [17] a loudspeaker used as a suspended piston is considered. It was demonstrated that a vibroacoustic NES can achieve very efficient noise reduction at low frequency. In both cases, the thin clamped structure has to be part of the frontier of the closed acoustic domain, one face (named the front face) is exposed to the primary acoustic field (to be controlled) whereas the other face (the rear face) radiates outside [16]. It results in a pressure difference applied to the membrane, which is necessary for TET. Neglecting the rear radiation impedance, the thin baffled structure is mainly coupled to the primary acoustic field.

In [16] a theoretical study was made on a system quite close to the one presented here, but it was much simpler (the NES was made of a bare membrane on the room's wall), the NES dynamics was simplified (purely passive, and no linear part in the membrane dynamics) and the numerical results were found for a very low damping (quality factor $Q = 36000$) that cannot be found in usual buildings. Moreover, like similar studies the rear face of the membrane needed to be exposed to a null acoustic field. In practice it means that it could not be enclosed and thus caused unwanted outward radiations preventing applications for acoustic enclosures.

In [18], a modified vibroacoustic NES was used on a resonant tube in order to provide noise reduction. The proposed NES named hybrid Electro-Acoustic nonlinear membrane absorber (EA-NES) is composed of a thin circular visco-elastic membrane with one face coupled to the acoustic field to be reduced and the other face enclosed. The enclosure includes a loudspeaker for the control of the acoustic pressure felt by the rear face of the membrane through proportional feedback control. It was shown experimentally that the EA-NES is able to perform resonance capture with the acoustic field, resulting in noise reduction by targeted energy transfer. Furthermore it was shown that the EA-NES provides a better noise attenuation in this setup than the classic vibroacousctic NES[15, 16], but in [18] there was no model of the dynamics of the experiment.

The objective of this paper is to investigate analytically and experimentally the performance of the EA-NES considering voltage and current driving mode of the control loudspeaker in realistic conditions. Unlike previous theoretical or experimental studies, the primary system where the acoustic field

is meant to be mitigated is an acoustic cavity mostly made of concrete walls. Indeed the enclosure of the EA-NES makes the membrane interact with the primary acoustic field without the need to be placed across the outer boundary and thus solves the problem of outward radiation. A simple three Degrees Of Freedom (DOF) model is developed coupling an electro-mechanical-acoustic model for the EA-NES with a model cavity representative of one of the acoustic modes. We investigated the targeted energy transfer occurring between the acoustic medium and the EA-NES during sinusoidal forced regimes. The predictions of this model is compared with the experimental data.

The paper is organized as follows. In Section 2, we start with a short description of the system under study and the experimental setup, then we describe each element of the acoustic system, considering first each substructure separately, and then modeling the coupled system. In Section 3, we study the forced responses to harmonic excitation. The responses are estimated with the complexification averaging method, and compared with results of direct numerical integration of the equations in time domain. In Section 4, we begin with a description of the experimental setup. Then, we check the stability analysis of the feedback loop and perform a frequency analysis under broadband excitation. In the last part we analyze the forced responses and their agreement with the model in the nonlinear regime, and we discuss the efficiency of the EA-NES.

2. System under study

The system under study is shown in Fig. 1. It is composed of an acoustic cavity that includes the EA-NES at the position M_{a} and a source loudspeaker at the position M_{S}. We are looking at the acoustic pressure at positions M_1, M_2 and M_3.

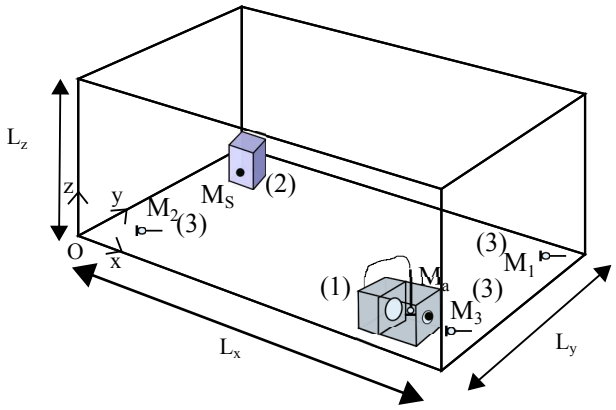

Figure 1: Schematic representation of the acoustic cavity: (1) EA-NES, (2) loudspeaker source, (3) microphones.

2.1. The hybrid electro-acoustic nonlinear membrane absorber (EA-NES)

2.1.1. Description of the setup

The same EA-NES as introduced in [18] is considered in this study. It is composed (see Fig. 2) of a plywood box with a circular (nonlinear) viscoelastic (latex) membrane clamped on one face. The clamped membrane with its supporting device is shown in Fig. 2(a). The device includes a sliding system used to apply a constant and permanent in-plan pre-stress to the membrane. An enclosed electrodynamic loudspeaker (BEYMA 8P300Fe/N

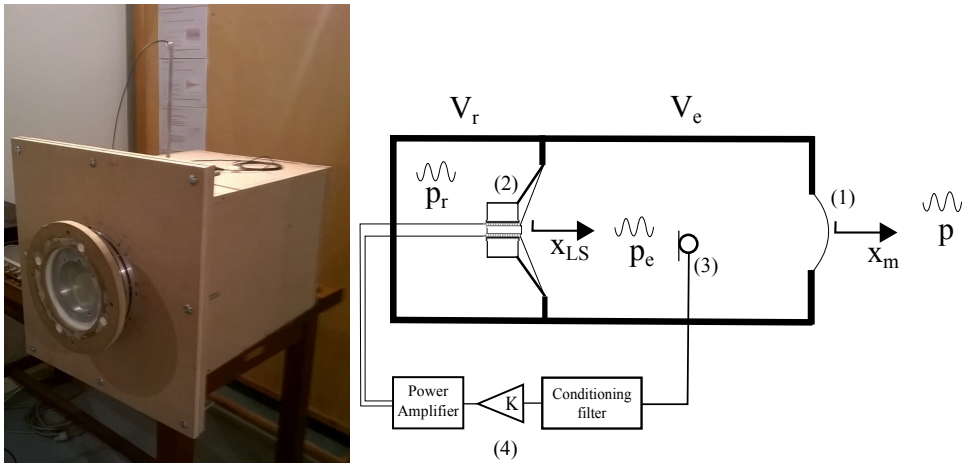

Figure 2: Picture and schematic representation of the hybrid electro-acoustic nonlinear absorber: (1) clamped membrane, (2) control loudspeaker, (3) control microphone, (4) amplifier with conditioning filter loop gain.

loudspeaker, 8 Inch) named "control loudspeaker" is mounted inside the box (see Fig. 2(b)). The coupling between the membrane and the control loudspeaker is ensured acoustically by the air in a coupling box of a volume V_e. The volume of the rear enclosure of the control loudspeaker is V_r. An active controller is used to perform a pressure reduction at the rear face of the membrane using the control loudspeaker in voltage or current driving mode. The controller is an analog feedback loop that reduces the pressure measured in the enclosure V_e by using a proportional gain K. The gain K is calibrated by feeding the power amplifier with a reference sinus of $0.1\,\mathrm{V}_{rms}$ and measuring its output level. The maximum value for K is limited by the stability of the loop and depends on the electrical driving mode. The maximum value of K before instability can be predicted thanks to the measurement of the open loop transfer, as described in [18].

The EA-NES is based on the conjugate functioning of three elements: (i) the clamped membrane that interacts with the acoustic field in order to provide noise attenuation in its non-linear range; (ii) the hood by which the EA-NES can work inside a surrounding acoustic field unlike previous developed NES; (iii) the feedback loop that reduces the pressure in the hood and allows to use a small hood volume and also to tune the stiffness and damping linear behavior of the EA-NES.

2.1.2. Equations of Motion

A simplified model is developed to address the properties of the device. The model is obtained by coupling the behaviors of the membrane and the control loudspeaker.

As explained in [15], a simplified model of the pre-stressed membrane motion can be formulated as a one DOF nonlinear oscillator

$$m_{\mathrm{m}}\ddot{x}_{\mathrm{m}}(t) + c_{1\mathrm{m}}\dot{x}_{\mathrm{m}}(t) + k_{1\mathrm{m}}x_{\mathrm{m}}(t) + g_{\mathrm{m}}(x_{\mathrm{m}}(t), \dot{x}_{\mathrm{m}}(t)) = \frac{S_{\mathrm{m}}}{2}\left(p_{\mathrm{e}}(t) - p(t)\right) \quad (1)$$

where x_{m} denotes the transverse displacement of the center of the membrane, $p_{\mathrm{e}}(t)$ denotes the acoustic pressure in the coupling box V_{e} and $p(t)$ is the acoustic pressure at the outer (front) surface of the membrane; $p(t)$ is considered here as the forcing term. The linear parameters are given by [15]

$$m_{\mathrm{m}} = \frac{\rho_{\mathrm{m}} h_{\mathrm{m}} S_{\mathrm{m}} + m_{\mathrm{a}}}{3}, \quad k_{1\mathrm{m}} = k_{0\mathrm{m}}\left(\frac{f_{1\mathrm{m}}}{f_{0\mathrm{m}}}\right)^2 \quad \text{and} \quad c_{1\mathrm{m}} = \eta k_{0\mathrm{m}} \qquad (2)$$

with

$$k_{0\mathrm{m}} = \frac{2\pi E h_{\mathrm{m}}^3}{3(1-\nu^2)R_{\mathrm{m}}^2} \quad \text{and} \quad f_{0\mathrm{m}} = \frac{1}{2\pi}\sqrt{\frac{1.015^4\pi^4 E h_{\mathrm{m}}^2}{12(1-\nu^2)\rho_{\mathrm{m}} R_{\mathrm{m}}^4}}. \qquad (3)$$

The nonlinear term is given by [15]

$$g_{\mathrm{m}}(x_{\mathrm{m}}, \dot{x}_{\mathrm{m}}) = k_{3\mathrm{m}}(x_{\mathrm{m}}^3 + 2\eta x_{\mathrm{m}}^2 \dot{x}_{\mathrm{m}}) \text{ with } \quad k_{3\mathrm{m}} = \frac{1}{2}\frac{8\pi E_{\mathrm{m}} h_{\mathrm{m}}}{3(1-\nu^2)R_{\mathrm{m}}^2} \qquad (4)$$

where ρ_{m} is the mass volume, ν the Poisson's coefficient and E the Young's modulus of the membrane (made here in latex), h_{m} is its thickness, R_{m} its radius and S_{m} its area. A mass term m_{a} has been added to include in the model the mass of the air column introduced by the sliding system. The coefficients $k_{1\mathrm{m}}$ and $k_{3\mathrm{m}}$ stand for the linear and nonlinear stiffness coefficients, respectively. As suggested and justified in [15], the coefficient $k_{3\mathrm{m}}$ was divided by 2 [19]. $f_{0\mathrm{m}}$ represents the resonance frequency of the membrane without pre-stress. The last two parameters $f_{1\mathrm{m}}$ ($\geq f_{0\mathrm{m}}$) and η (> 0) have to be adjusted. The first one is related to the pre-tension applied to the membrane. When no pre-tension is considered, $f_{1\mathrm{m}} = f_{0\mathrm{m}}$. The second parameter η characterizes the damping.

Considering now the control loudspeaker, assuming a linear behavior, the equations of motion follow from Newton's second and Kirchhoff's laws as

$$\begin{aligned} m_{\mathrm{ms}}\ddot{x}_{\mathrm{LS}}(t) + c_{\mathrm{ms}}\dot{x}_{\mathrm{LS}}(t) + k_{\mathrm{ms}}x_{\mathrm{LS}}(t) &= Bli_{\mathrm{LS}}(t) + S_{\mathrm{LS}}\left(p_{\mathrm{r}}(t) - p_{\mathrm{e}}(t)\right), \quad (5) \\ u_{\mathrm{LS}}(t) &= R_{\mathrm{e}}i_{\mathrm{LS}}(t) + Bl\dot{x}_{\mathrm{LS}}(t) \qquad (6) \end{aligned}$$

where $x_{\mathrm{LS}}(t)$ is the diaphragm displacement, $u_{\mathrm{LS}}(t)$ the voltage applied at the electrical terminals of the control loudspeaker, $i_{\mathrm{LS}}(t)$ the electrical current flowing through the voice coil and $p_{\mathrm{r}}(t)$ the acoustic pressure in the rear enclosure. The coefficients m_{ms}, c_{ms} and k_{ms}^{-1} represent the moving mass, the mechanical damping and the mechanical compliance accounting for the elastic surround suspension and the spider. Bl is the force factor of the transducer, S_{LS} is the effective radiation area of the loudspeaker and R_{e} is

DC resistance (the inductance has been neglected) of the voice coil. All the parameters used in this model are commonly denoted as a part of the Thiele-Small parameters of the loudspeaker.

Equations (1) and (5) are coupled by writing that the acoustic pressures $p_{\mathrm{e}}(t)$ and $p_{\mathrm{r}}(t)$ are related to the relative variation of the volumes V_{e} and V_{r} due to the motion of the membrane and the diaphragm of the control loudspeaker as

$$p_{\mathrm{e}}(t) \;=\; \frac{\rho_{\mathrm{a}} c_0^2}{V_{\mathrm{e}}}(S_{\mathrm{LS}} x_{\mathrm{LS}}(t) - \frac{S_{\mathrm{m}}}{2} x_{\mathrm{m}}(t)) \text{ and } p_{\mathrm{r}}(t) \;=\; -\frac{\rho_{\mathrm{a}} c_0^2}{V_{\mathrm{r}}} S_{\mathrm{LS}} x_{\mathrm{LS}}(t) \qquad (7)$$

where ρ_{a} is the density of the air and c_0 is the sound wave velocity in the air.

Finally the feedback loop using the electric terminals of loudspeaker as input is defined as

$$u_{\mathrm{LS}}(t) = -K S_{\mathrm{mic}} p_{\mathrm{e}}(t) \qquad (8)$$

when the loudspeaker is driven by voltage-output power amplifier and

$$i_{\mathrm{LS}}(t) = -K S_{\mathrm{mic}} p_{\mathrm{e}}(t) \qquad (9)$$

when the loudspeaker is driven by current-output power amplifier. In Eqs. (8) and (9), S_{mic} denotes the microphone sensibility and K the control gain of the feedback loop. Note that a minus sign has been included in the model to ensure that a positive gain K leads to a reduction of the pressure $p_{\mathrm{e}}(t)$ in the volume V_{e} as observed for the step up.

Combining Eqs. (1) to (9) and eliminating the variables $p_{\mathrm{e}}(t)$, $u_{\mathrm{LS}}(t)$,$i_{\mathrm{LS}}(t)$ and $p_{\mathrm{r}}(t)$, results in a 2-DOF nonlinear system of the form

$$\mathbf{M}\ddot{\mathbf{X}}(t) + \mathbf{C}\dot{\mathbf{X}}(t) + \mathbf{K}\mathbf{X}(t) + \mathbf{B} g_{\mathrm{m}}(x_{\mathrm{m}}(t), \dot{x}_{\mathrm{m}}(t)) = -\mathbf{B}\frac{S_{\mathrm{m}}}{2} p(t) \qquad (10)$$

where $\mathbf{X}(t) = (x_{\mathrm{m}}(t), x_{\mathrm{LS}}(t))^T$, $\mathbf{B} = (1,0)^T$,

$$\mathbf{M} = \begin{bmatrix} m_{\mathrm{m}} & 0 \\ 0 & m_{\mathrm{ms}} \end{bmatrix}, \quad \mathbf{C} = \begin{bmatrix} c_{1\mathrm{m}} & 0 \\ 0 & c_{\mathrm{ms}} + \dfrac{\alpha_{\mathrm{ms}}(Bl)^2}{aa} \end{bmatrix} \quad \text{and} \tag{11}$$

$$\mathbf{K} = \begin{bmatrix} k_{1\mathrm{m}} + \dfrac{\rho_{\mathrm{a}} c_0^2}{V_{\mathrm{e}}} \dfrac{S_{\mathrm{m}}^2}{4} & -\dfrac{\rho_{\mathrm{a}} c_0^2}{V_{\mathrm{e}}} \dfrac{S_{\mathrm{m}}}{2} S_{\mathrm{LS}} \\ -\dfrac{\rho_{\mathrm{a}} c_0^2}{V_{\mathrm{e}}} \dfrac{S_{\mathrm{m}}}{2} (\dfrac{Bl}{aa} \mathrm{K} S_{\mathrm{mic}} + S_{\mathrm{LS}}) & k_{\mathrm{ms}} + \dfrac{\rho_{\mathrm{a}} c_0^2}{V_{\mathrm{e}}} S_{\mathrm{LS}} (\dfrac{Bl}{aa} K S_{\mathrm{mic}} + S_{\mathrm{LS}} \dfrac{V_{\mathrm{e}} + V_{\mathrm{r}}}{V_{\mathrm{r}}}) \end{bmatrix} \tag{12}$$

with $aa = 1 - \alpha_{\mathrm{ms}} + \alpha_{\mathrm{ms}} R_{\mathrm{e}}$. The parameter α_{ms} has been introduced to characterize the output power amplifier mode of the loudspeaker. If $\alpha_{\mathrm{ms}} = 1$, the loudspeaker is assumed driven by a voltage output power amplifier (Eq. (8)) whereas if $\alpha_{\mathrm{ms}} = 0$, the loudspeaker is driven by a current output power amplifier (Eq. (9)).

Independently of the control loop strategy, the mass $\mathbf{M}$ and the damping $\mathbf{C}$ matrices are always diagonal with positive terms whereas the stiffness matrix $\mathbf{K}$ is not symmetric except if $K = 0$ (passive system). When the loudspeaker is driven by a current output power amplifier only the stiffness matrix $\mathbf{K}$ is affected and the damping effect is only due to the mechanical system whereas when the loudspeaker is driven by a voltage output power amplifier the stiffness matrix $\mathbf{K}$ and the damping matrix $\mathbf{C}$ are affected by the electrical resistance. In this case, the corrective term in the damping matrix $\mathbf{C}$ is equal to $\dfrac{(Bl)^2}{R_{\mathrm{e}}}$ and, in practice, it dominates over the mechanical damping constant c_{ms}. The corrective terms in the stiffness matrix $\mathbf{K}$ due to the control loop are proportional to $\dfrac{Bl}{aa} K S_{\mathrm{mic}}$ reducing to $\dfrac{Bl}{R_{\mathrm{e}}} K S_{\mathrm{mic}}$ when $\alpha_{\mathrm{ms}} = 1$ and to $BlKS_{\mathrm{mic}}$ when $\alpha_{\mathrm{ms}} = 0$ and showing that choosing the gain $\dfrac{K}{R_{\mathrm{e}}}$ when the loudspeaker is driven by a current output power amplifier

is equivalent in terms of stiffness matrix to choosing the gain K when the loudspeaker is driven by a voltage output power amplifier.

2.2. Primary system: acoustic room

The primary system is a rectangular shaped room with dimension L_x, L_y and L_z (see Fig. 1). We assume that all the walls of the room are rigid. The equation of motion as a one DOF system is obtained by performing a Rayleigh-Ritz reduction taking account of one mode on the following wave equation (see for example [16])

$$\begin{aligned} \frac{1}{c_0^2}\frac{\partial^2}{\partial t^2}p(M,t) - \Delta p(M,t) &= -\rho_{\mathrm{a}}(\delta_{M_{\mathrm{a}}}(M)\dot{q}_{\mathrm{m}}(t) + \delta_{M_{\mathrm{S}}}(M)\dot{q}_{\mathrm{S}}(t)) \text{ on } \Omega, \quad (13) \\ \partial_n p(M,t) &= 0 \text{ on } \partial\Omega \quad (14) \end{aligned}$$

where Ω is the internal volume of the room and $\partial\Omega$ is the surface of room. The first term of the right hand side of Eq. (13) characterizes the coupling with the EA-NES considering the volumetric flow rate $q_{\mathrm{m}}(t)$ resulting from the vibration of the membrane as

$$q_{\mathrm{m}}(t) = -\frac{S_{\mathrm{m}}}{2}\dot{x}_{\mathrm{m}}(t). \quad (15)$$

The minus sign results from the vector direction used to represent the motion of the membrane (see Fig. 2). The last term in Eq. (13) characterizes the acoustic source inside the room as a point flow source with the volumetric flow $q_{\mathrm{S}}(t)$.

Considering the mode marked by the integers (l,m,n) defined by the frequency ω_{lmn} and the mode shape $\Phi_{lmn}(x,y,z)$ as

$$\omega_{lmn} = c_0\pi\sqrt{\frac{l^2}{L_x^2}+\frac{m^2}{L_y^2}+\frac{n^2}{L_z^2}} \text{ and } \Phi_{lmn}(x,y,z) = \cos\frac{l\pi x}{L_x}\cos\frac{m\pi y}{L_y}\cos\frac{n\pi z}{L_z},$$

and approximating the acoustic pressure as

$$p(M,t) = \Phi_{lmn}(M)p(t), \tag{16}$$

Eqs. (13) and (14) reduce to

$$m_{lmn}\ddot{p}(t) + c_{lmn}\dot{p}(t) + k_{lmn}p(t) = \rho_{\mathrm{a}}^2 c_0^2(\Phi_{lmn}(M_{\mathrm{a}})\frac{S_{\mathrm{m}}}{2}\ddot{x}_{\mathrm{m}}(t) - \Phi_{lmn}(M_{\mathrm{S}})\dot{q}_{\mathrm{S}}(t)) \tag{17}$$

where $m_{lmn} = m_{\mathrm{C}}((2-\delta_0(l)(2-\delta_0(m))(2-\delta_0(n))))^{-1}$ and $k_{lmn} = m_{lmn}\omega_{lmn}^2$ with $m_{\mathrm{C}} = \rho_{\mathrm{a}}L_xL_yL_z$ (the mass of the air inside the cavity). The acoustic damping gives a viscous term $c_{lmn} = \sqrt{m_{lmn}k_{lmn}}Q_{lmn}^{-1}$ with Q_{lmn} the quality factor associated to the corresponding mode.

Finally for the sake of simplicity, we do not model the loudspeaker source and its power supply. We assume that the volumetric flow source is of the form

$$q_{\mathrm{S}}(t) = \sqrt{2}A_{\mathrm{S}}\cos(\omega_{\mathrm{S}}t) \tag{18}$$

where $\omega_{\mathrm{S}}(=2\pi f_{\mathrm{S}})$ denotes the excitation frequency and A_{S} the RMS value of the excitation amplitude.

2.3. The final dimensional and non-dimensional 3*-DOF systems*

The final dimensional model is obtained by grouping Eq. (17) with Eq. (10). Introducing the non dimensional quantity by normalizing the acoustic pressure $p(t)$ with $\rho_{\mathrm{a}}c_0^2$, normalizing the time with the resonance frequency ω_{lmn} of the cavity and resealing the final dimensional system with the parameter ϵ as

$$\tilde{p}(t) = p(t)/(\rho_{\mathrm{a}}c_0^2),\ \tilde{t} = \omega_{lmn}t \text{ and } \epsilon = \frac{m_{\mathrm{m}}}{m_{lmn}}, \tag{19}$$

we obtain the following non-dimensional 3-DOF system (after omission of tilde)

$$\ddot{p} + \epsilon\lambda_{\rm p}\dot{p} + p - \epsilon\mu_{\rm p}\ddot{x}_{\rm m} = -\epsilon\beta(1+\epsilon\bar{\sigma})\sin((1+\epsilon\bar{\sigma})t), \tag{20}$$

$$\epsilon\ddot{x}_{\rm m} + \epsilon\lambda_{\rm m}\dot{x}_{\rm m} + \epsilon\lambda_{\rm 2m}x_{\rm m}^2\dot{x}_{\rm m} + \epsilon\bar{k}_{11}x_{\rm m} + \epsilon\bar{k}_{12}x_{\rm LS} + \epsilon\bar{k}_{\rm 3m}x_{\rm m}^3 + \epsilon\mu_{\rm m}p = 0, \tag{21}$$

$$\epsilon\gamma_{\rm LS}\ddot{x}_{\rm LS} + \epsilon\lambda_{\rm LS}\dot{x}_{\rm LS} + \epsilon\bar{k}_{21}x_{\rm m} + \epsilon\bar{k}_{22}x_{\rm LS} = 0 \tag{22}$$

where now the dot denotes the differentiation with respect to the new time variable,

$$\lambda_p = \tfrac{c_{lmn}}{m_{\rm m}\omega_{lmn}},\ \mu_{\rm p} = \tfrac{\Phi_{lmn}(M_{\rm a})\rho_{\rm a}S_{\rm m}}{2m_{\rm m}},\ \bar{k}_{11} = \tfrac{k_{11}}{m_{\rm m}\omega_{lmn}^2},\ \bar{k}_{12} = \tfrac{k_{12}}{m_{\rm m}\omega_{lmn}^2}, \tag{23}$$

$$\bar{k}_{21} = \tfrac{k_{21}}{m_{\rm m}\omega_{lmn}^2},\ \bar{k}_{22} = \tfrac{k_{22}}{m_{\rm m}\omega_{lmn}^2},\ \lambda_{\rm m} = \tfrac{c_{11}}{m_{\rm m}\omega_{lmn}},\ \lambda_{\rm 2m} = \tfrac{2\eta k_{\rm 3m}}{m_{\rm m}\omega_{lmn}}, \tag{24}$$

$$\bar{k}_{\rm 3m} = \tfrac{k_{\rm 3m}}{m_{\rm m}\omega_{lmn}^2},\ \mu_{\rm m} = \tfrac{\Phi_{lmn}(M_{\rm a})\rho_{\rm a}c_0^2S_{\rm m}}{2m_{\rm m}\omega_{lmn}^2},\ \gamma_{\rm LS} = \tfrac{m_{\rm LS}}{m_{\rm m}},\ \lambda_{\rm LS} = \tfrac{c_{22}}{m_{\rm m}\omega_{lmn}}, \tag{25}$$

$$\beta = \tfrac{\Phi_{lmn}(M_{\rm S})\rho_{\rm a}\sqrt{2}A_{\rm S}}{m_{\rm m}\omega_{lmn}} \text{ and } \bar{\sigma} = \tfrac{\omega_{\rm S}-\omega_{lmn}}{\omega_{lmn}}\tfrac{m_{lmn}}{m_{\rm m}} \tag{26}$$

with k_{ij} (respectively c_{ij}) denotes the ij-component of the matrix $\mathbf{K}$ (respectively $\mathbf{C}$).

2.4. About the numerical values for the parameters of the models

The biggest size, L_x, of the room was $L_x = 3.928$ m given (with $\rho_{\rm a} = 1.17$ kg m^{-1} and $c_0 = 344.5$ m s^{-1}) for the $(1,0,0)$-mode the frequency $f_{100} \simeq 43.8$ Hz in good agreement with the measured one. The quality factor was fixed as $Q_{100} = 133$ the measured one.

The volumes of the two main closed boxes of the EA-NES were $V_{\rm e} = 0.018225$ m^3 and $V_{\rm r} = 0.0248$ m^3. The membrane parameters were: radius $R_{\rm m} = 0.05$ m, thickness $h_{\rm m} = 0.00024$ m and material parameters defined by $\rho_{\rm m} = 980.$ kg.m^{-3}, $\nu = 0.49$, $E = 1500000.$ Pa. The free parameters of the

membrane model, m_{a}, $f_{1\mathrm{m}}$ and η, were adjusted as $m_{\mathrm{a}} = 0.00011$ kg (about 15% of the mass membrane), $f_{1\mathrm{m}} = 2.5$ Hz (corresponding to moderate pretension) and $\eta = 0.001$ (light damping). These numerical values were chosen in accordance with numerical/experimental studies proposed in [15, 20, 16].

The Thiele-Small parameters of the control loudspeaker were measured given the following parameter values: $m_{\mathrm{ms}} = 19.4\ 10^{-3}$ kg, $c_{\mathrm{ms}} = 1.7$ Nsm^{-1}, $k_{\mathrm{ms}} = 2834.9$ Nm^{-1}, $S_{\mathrm{LS}} = 0.022$ m^2, $R_{\mathrm{e}} = 6.6\ \Omega$, $Bl = 9.21$ NA^{-1}. The resonance frequency of the driver part is 60.8 Hz and the effective diaphragm area is six time larger than the effective latex membrane.

A microphone G.R.A.S. 40BH with a sensitivity $S_{\mathrm{mic}} = 0.46$ mVPa^{-1} was used as the control microphone.

The source loudspeaker was positioned at M_{S} with coordinates $x_{M_{\mathrm{S}}} = 0.3$ m, $y_{M_{\mathrm{S}}} = 2.75$ m and $z_{M_{\mathrm{S}}} = 0.5$ m. The EA-NES was positioned at M_{a} with coordinates $x_{M_{\mathrm{a}}} = 3.65$ m, $y_{M_{\mathrm{a}}} = 0.35$ m and $z_{M_{\mathrm{a}}} = 0.35$ m. The microphone M_1 (respectively M_2 and M_3) was positioned at $(3.65, 2.8, 0.2)$ (respectively $(0.5, 0.2, 0.2)$ and $(3.65, 0.2, 0.2)$). To maximize the modal sensitivity they are located in the corners and near the floor, reducing the perturbation due to the ceiling pyramidal shape.

To characterize completely the behavior of the EA-NES, we have to choose the driving mode of the control loudspeaker (current ($\alpha_{\mathrm{ms}} = 0$) or voltage ($\alpha_{\mathrm{ms}} = 1$)) and the gain value K.

3. Asymptotic analysis

In this section we assume that $\epsilon << 1$ i.e the mass of the membrane is small with respect to the mass of the primary system ($\epsilon = 5 \cdot 10^{-5}$ with

parameter values as described in Section 2.4). We assume also that the parameters λ_p, $\mu_{\rm p}$, $\bar{k}_{11}$, $\bar{k}_{12}$, $\bar{k}_{21}$, $\bar{k}_{22}$, $\lambda_{\rm m}$, $\lambda_{\rm 2m}$, $\bar{k}_{\rm 3m}$, $\mu_{\rm m}$, $\gamma_{\rm LS}$, $\lambda_{\rm LS}$, β, and $\bar{\sigma}$ are of order 0(1).

The objective of the asymptotic analysis is to characterize analytically the forced responses of Eqs. (20) to (22) near the resonance frequency of the primary system.

We follow the same methodology as proposed in [21]. The method combines the complexification averaging procedure (as described in [22]) and an asymptotic analysis which is here based on the framework of the geometric singular perturbation theory [23, 24].

The complexification consists in introducing the change of variables

$$\psi_1 = \dot{p} + jp,\ \psi_2 = \dot{x}_{\rm m} + jx_{\rm m} \text{ and } \psi_3 = \dot{x}_{\rm LS} + jx_{\rm LS} \tag{27}$$

where $j^2 = -1$ and writing the complex variables ψ_i as

$$\psi_i = \phi_i e^{jt} \text{ for } i = 1, 2, 3 \tag{28}$$

where the ϕ_i are the complex (assumed) slow modulated amplitude of the fast component e^t.

Substituting Eqs. (27) and (28) into Eqs. (20) to (22) and averaging over one period of frequency 1 yields to a system of equations describing the behavior of the slow complex amplitudes ϕ_i as

$$\dot{\phi}_1 = \epsilon f_1(\phi_1, \phi_2, \phi_3), \tag{29}$$

$$\dot{\phi}_2 = f_2(\phi_1, \phi_2, \phi_3, \epsilon), \tag{30}$$

$$\dot{\phi}_3 = f_3(\phi_1, \phi_2, \phi_3, \epsilon) \tag{31}$$

where

$$
\begin{aligned}
f_1(\phi_1,\phi_2,\phi_3) &= \frac{j}{8}(4\beta + (4j\lambda_{\rm p} - 8\bar{\sigma} + 4\mu_{\rm m}\mu_{\rm p})\phi_1 + 4\mu_{\rm p}(j\lambda_{\rm m} + \bar{k}_{11})\phi_2 \\
&\quad +4\bar{k}_{12}\mu_{\rm p}\phi_3 + (3\bar{k}_{3{\rm m}}\mu_{\rm p} + j\lambda_{2{\rm m}}\mu_{\rm p})|\phi_2|^2\phi_2), \qquad (32) \\
f_2(\phi_1,\phi_2,\phi_3,\epsilon) &= \frac{j}{8}(4\mu_{\rm m}\phi_1 + (4\bar{k}_{11} + 4j\lambda_{\rm m} - 8\bar{\sigma}\epsilon - 4)\phi_2 + 4\bar{k}_{12}\phi_3 \\
&\quad +(3\bar{k}_{3{\rm m}} + j\lambda_{2{\rm m}})|\phi_2|^2\phi_2), \qquad (33) \\
f_3(\phi_1,\phi_2,\phi_3,\epsilon) &= \frac{j}{2\gamma_{\rm LS}}\left(\bar{k}_{21}\phi_2 + (\bar{k}_{22} - 2\bar{\sigma}\epsilon\gamma_{\rm LS} - \gamma_{\rm LS} + j\lambda_{\rm LS})\phi_3\right). \qquad (34)
\end{aligned}
$$

Eqs. (29) to (31) have a classic form of singular perturbation equations (slow-fast system), which is more evident by switching from the fast time scale t to the slow time scale $\tau = \epsilon t$ as

$$
\begin{aligned}
\phi_1' &= f_1(\phi_1,\phi_2,\phi_3), \qquad (35) \\
\epsilon\phi_2' &= f_2(\phi_1,\phi_2,\phi_3,\epsilon), \qquad (36) \\
\epsilon\phi_3' &= f_3(\phi_1,\phi_2,\phi_3,\epsilon) \qquad (37)
\end{aligned}
$$

where $(.)' = d/d\tau$ and $\phi(\tau) = \phi(t = \tau/\epsilon)$, since now the small parameter affects the first derivative of some slow-fast state variables (ϕ_2 and ϕ_3 here).

Stating $\epsilon = 0$, the following subsystems are derived from Eqs. (29) to (31) and Eqs. (35) to (37) respectively

$$
\begin{aligned}
\dot{\phi}_1 &= 0, \qquad (38) \\
\dot{\phi}_2 &= f_2(\phi_1,\phi_2,\phi_3,0), \qquad (39) \\
\dot{\phi}_3 &= f_3(\phi_1,\phi_2,\phi_3,0) \qquad (40)
\end{aligned}
$$

which is the fast subsystem, and

$$\begin{aligned} \phi_1' &= f_1(\phi_1, \phi_2, \phi_3), && (41) \\ 0 &= f_2(\phi_1, \phi_2, \phi_3, 0), && (42) \\ 0 &= f_3(\phi_1, \phi_2, \phi_3, 0) && (43) \end{aligned}$$

which is the slow subsystem.

In the following sections the geometric singular perturbation theory is used to describe the dynamics of the full system Eqs. (29) to (31) (and Eqs. (35) to (37)) for $0 < \epsilon << 1$ from the analysis of the fast, Eqs. (38) to (40), and slow, Eqs. (41) to (43), subsystems.

3.1. The Slow Invariant Manifold

At slow time, the motions of the slow subsystem, Eqs. (41) to (43), take place in the so-called Slow Invariant Manifold (SIM) defined by the algebraic equations (42) and (43) as

$$CM := \left\{ (\phi_1, \phi_2, \phi_3) \in \mathbb{C}^3 \;\middle|\; f_2(\phi_1, \phi_2, \phi_3, 0) = 0, f_3(\phi_1, \phi_2, \phi_3, 0) = 0 \right\}. \quad (44)$$

The points of the SIM are also fixed points for the fast subsystem (fast time) (Eqs. (38) to (40)).

Substituting Eq. (43) into Eq. (42), the SIM can take the following form

$$\begin{aligned} \phi_1 &= \phi_2 F(|\phi_2|), && (45) \\ \phi_3 &= \frac{\bar{k}_{21}}{\gamma_{\mathrm{LS}} - \bar{k}_{22} - j\lambda_{\mathrm{LS}}} \phi_2 && (46) \end{aligned}$$

where the complex function F of a real variable is defined as $F(x) = F_{\mathrm{R}}(x) +$

$jF_{\rm I}(x)$ with

$$F_{\rm R}(x) = \frac{\bar{k}_{12}\bar{k}_{21}(\bar{k}_{22}-\gamma_{\rm LS})}{\mu_{\rm m}\left(\left(\bar{k}_{22}-\gamma_{\rm LS}\right)^2+\lambda_{\rm LS}^2\right)}+\frac{1-\bar{k}_{11}}{\mu_{\rm m}}-\frac{3}{4}\frac{\bar{k}_{3\rm m}}{\mu_{\rm m}}x^2, \quad (47)$$

$$F_{\rm I}(x) = -\frac{\bar{k}_{12}\bar{k}_{21}\lambda_{\rm LS}}{\mu_{\rm m}(\left(\bar{k}_{22}-\gamma_{\rm LS}\right)^2+\lambda_{\rm LS}^2)}-\frac{\lambda_{\rm m}}{\mu_{\rm m}}+\frac{1}{4}\frac{\lambda_{2\rm m}}{\mu_{\rm m}}x^2. \quad (48)$$

It is convenient to characterize the CM in the real domain. To achieve this, polar coordinates are introduced as

$$\phi_i = N_i e^{j\theta_i} \text{ for } i=1,2,3 \quad (49)$$

and we compute successively the module and the argument of Eqs. (45) and (46) that lies to

$$N_1^2 = N_2^2(F_{\rm R}(N_2)^2+F_{\rm I}(N_2)^2), \quad (50)$$

$$N_3 = |\frac{\bar{k}_{21}}{\gamma_{\rm LS}-\bar{k}_{22}-j\lambda_{\rm LS}}|N_2, \quad (51)$$

$$\theta_1 = \theta_2+\arctan(\frac{F_{\rm I}(N_2)}{F_{\rm R}(N_2)}, \quad (52)$$

$$\theta_3 = \theta_2+\arg(\frac{\bar{k}_{21}}{\gamma_{\rm LS}-\bar{k}_{22}-j\lambda_{\rm LS}}). \quad (53)$$

The SIM is characterized by as a one-dimensional parametric curve (N_2, N_1, N_3) evolving in $\mathbb{R}^{+^3}$. A typical critical manifold is plotted in Fig. 3(a)(red curve). Due to the linear relation (51), its form is mainly given by its projection on the (N_2, N_1)-plane (see Fig. 3(a)(blue continuous curve)) which corresponds to Eq. (50). The expression of the SIM is similar to that obtained in [21] to study harmonic forced linear system. As in [21], the SIM do not depend on the excitation level, the damping of the primary system and the coupling term $\mu_{\rm p}$.

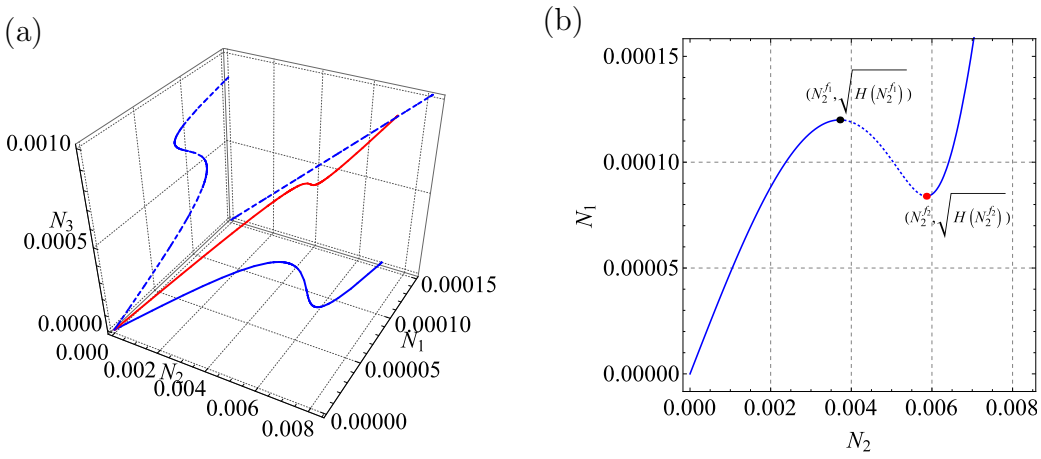

Figure 3: Typical slow invariant manifold: (a) in (N_2, N_1, N_3)-space (red curve) and (b) in (N_2, N_1)-plane (blue curve) with fold points (maximum-black, minimum-red) and unstable zone (dotted curve).

The form of the SIM is characterized by the local extrema of the function $H(x) = x^2(F_{\mathrm{R}}(x)^2 + F_{\mathrm{I}}(x)^2)$ in the (N_2, N_1)-plane (see Eq. (50)). Local extrema are equivalently defined as the positive root of the derivative of H as a function of x^2 resulting in a polynomial of degree 2 admitting zero, one or two positive roots.

The stability of each point of the SIM as a fixed point of the fast subsystem (38-40) (fast time) can be determined. It can be shown that the condition of stability is equivalent to

$$H'(N_2) > 0 \tag{54}$$

where $H'(x) = dH(x)/dx$. Hence when two local extrema exist for H, denoted N_2^{f1} and N_2^{f2}, these local extrema define two points $(N_2^{f1}, \sqrt{H(N_2^{f1})}$ and $(N_2^{f2}, \sqrt{H(N_2^{f2})}$ called fold points where stability change occurs. Fig. 3 corresponds to a case where two fold points exist, see Fig. 3(b), and the stability zones are also reported. Such a SIM structure may give rise to Strongly

Modulated Responses (SMR)[21].

Formulating conditions on the model parameters for getting two positive roots would result in large expressions which would be difficult to manipulate. Some numerical parametric study will only be discussed in Section 3.2.

A characterization of the fixed points and folded singularities of the slow-flow from the slow subsystem (41)-(43) is given Appendix Appendix A including conditions on the excitation level β for allowing SMR.

3.2. Parametric study of the current and voltage gain K

The SIMs are plotted Fig. 4(a) from Eq. (50) in the (N_2, N_1)-plane using the numerical values discussed Section 2.4 and for different values of gain K for current control. The associated plot, Fig. 4(b), represents the critical excitation level $\beta_{\rm cr}$ versus K from Eq. (A.22) for the same conditions. For small values of K, the SIM does not show fold points whereas for $K > K^{\rm rel} \approx 2.01$ (see Fig. 4(b)), two fold points exist (see Fig. 4(a)). Hence $K^{\rm rel}$ defines the threshold gain from which SMRs can take place if $\beta > \beta_{\rm cr}^{\rm rel}$ (i.e if the excitation level is sufficient high). The critical excitation level $\beta_{\rm cr}^{\rm rel}$ characterizes a threshold in terms of excitation level. Equivalently a threshold can be defined in terms of N_1-amplitude (primary system) by $\sqrt{H(N_2^{f_1})}$ (the ordinates of the fold points, see Fig. 4(a)(black markers)). Both thresholds increase with the gain K.

Figure 5 represents the same quantities but obtained for different values of gain K for voltage control. Here also for small values of K, the SIM does not show fold points whereas for $K > K^{\rm rel} \approx 27.18 R_{\rm e}$ (see Fig. 5(b)), two fold points exist (see Fig. 5(a)). Contrary to the current control, the excitation level threshold slowly decreases and the N_1-amplitude level threshold slowly

increases when the gain K increases. Finally the thresholds associated to the voltage control are greater than the thresholds associated to the current control.

They give an order of magnitude for the excitation level needed in the unstable region, in view of setting the experimental conditions.

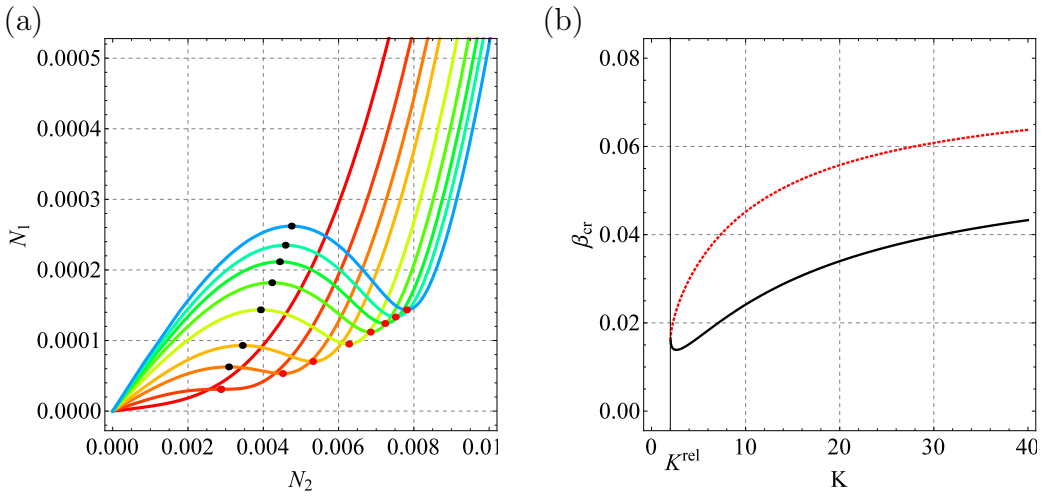

Figure 4: System with EA-NES driven by current: (a) Slow invariant manifold with fold points (maximum-black, minimum-red) for $K = 0$, K^{rel}, 4, 6, 10, 14, 18, 22 and 28 from the red curve ($K = 0$) to the blue curve ($K = 30$). (b) Critical values β_{cr} versus K: the dotted red curve corresponds to the red fold points whereas the continuous black curve corresponds to the black fold points ($K^{\text{rel}} \simeq 2.01$).

Figure 6 gives an example of the action of the EA-NES. We focus on EA-NES driven by current with $K = 7.5$ ($> K^{\text{rel}}$) and $\beta = 0.032$ ($> \beta_{\text{cr}}$). The acoustic pressure amplitude at point M_3 obtained with the adimensional model Eqs. (20) to (22) and the asymptotic analysis Eq. (A.13) are compared in Fig. 6 (a). Also plotted are the response of the primary system showing the efficiency of the EA-NES. It is slightly shifted to lower frequencies due to the absence of the linear part of the NES in the model of the room. The

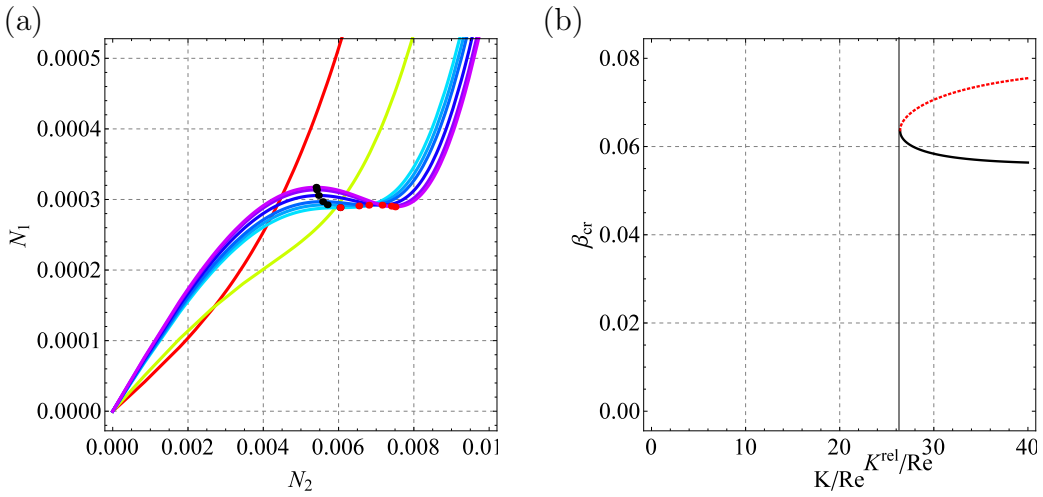

Figure 5: System with EA-NES driven by voltage: (a) Slow invariant manifold with fold points (maximum-black, minimum-red) with $K/R_e = 0$, 10, K^{rel}/R_e, 28, 30, 34, 38, and 40 from the red curve ($K/R_e = 0$) to the violet curve ($K/R_e = 40$). (b) Slow invariant values β_{cr} versus K/R_e: the dotted red curve corresponds to the red fold points whereas the continuous black curve corresponds to the black fold points ($K^{rel}/R_e \simeq 27.18$).

differential models were solved using ©Mathematica ordinary differential equations solver NDSolve (with the choice Automatic for the option Method) with the trivial equilibrium point as initial conditions. In the area of the stable periodic solutions, the asymptotic approximation matches very well with the integrated solution. In the unstable area, the integrated solution has a low amplitude compared to the response without EA-NES. This reduction is what the EA-NES is aimed at.

When the periodic solution is unstable, the system can exhibit SMR as observed Fig. 6 (b) for $f_S = 44.2$ Hz. The time response obtained from Eq. (20-22) is plotted in the (N_2, N_1)-plane. It oscillates around the unstable range.

These observations show that the EA-NES we study should be able to

reduce significantly the sound level in the room. These observations give also an indication about the source level and frequency around which the experiments should be done.

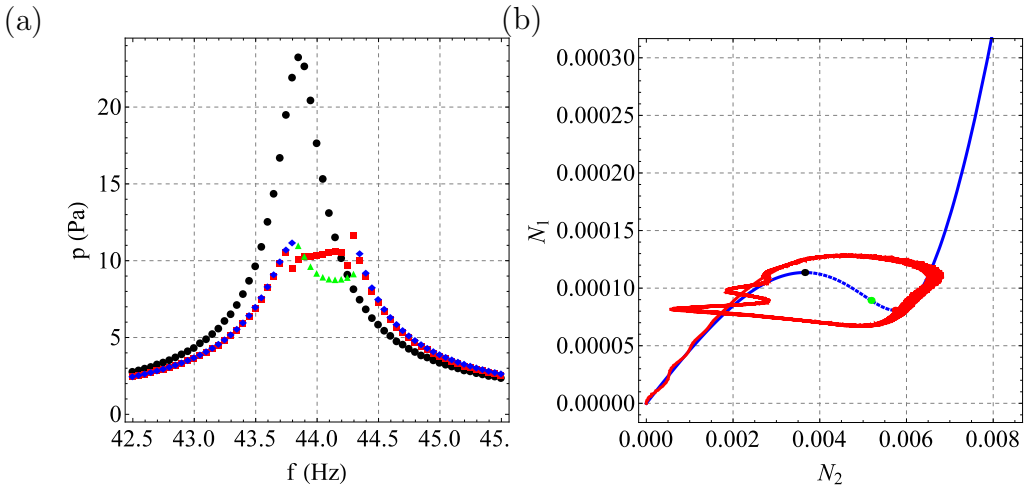

Figure 6: System with EA-NES driven by current with $K = 7.5$ and $A_s = 0.136$ ($\beta = 0.032$): (a) Forced response (acoustic pressure) at point M_3: primary system without NES (black dots), Eq. (20-22) (red squares), and stable (blue diamonds) and unstable (green triangles) fixed points obtained from Eq. (A.13). (b) Time responses (red curves) obtained from Eq. (20-22) in the (N_2, N_1)-plan for $f_S = 44.2$ Hz with the fold points (maximum-black and minimum-red markers) and the unstable fixed point (green marker).

4. Experimental study

4.1. Setup and primary analysis

The experiments were conducted in a concrete parallelepipedic room, except for the ceiling which has the shape of a shortened pyramid covered by a thick wooden floor as it can be seen in Fig. 7(a). A complete description can be founding in [25]. The size of the room is $L_x = 3.928$ m and $L_y = 3.05$ m with height from $L_z = 2.4$ m to 2.7 m. The source loudspeaker (an Electro Voice ELX118), the EA-NES and the microphones (a G.R.A.S 40BH at M_1, a G.R.A.S 40PR at M_2 and a G.R.A.S AF at M_3) were positioned as shown Fig. 1 and detailed in Section 2.4.

During a measurement, a target voltage signal e(t) from a generator (not shown in Fig. 1) and a power amplifier TIRA, BAA120 (not shown in Fig. 1) provide an input current signal to the source loudspeaker operating in current-feedback control mode. The responses of the system are recorded simultaneously using a multi-channel analyzer/recorder OROS, OR38 (not shown in Fig. 1): the acoustic pressures at M_1, M_2 and M_3, the acoustic pressure $p_{\mathrm{e}}(t)$ inside the EA-NES and the displacement at the center of the membrane of the EA-NES measured with an optical sensor Keyence LK-G152 (not shown in Fig. 1). Also recorded are the control loudspeaker current $i_{\mathrm{LS}}(t)$ and voltage $u_{\mathrm{LS}}(t)$ responses and the source loudspeaker current $i_s(t)$ and voltage $e_s(t)$ responses. The sampling frequency is fs = 8192 Hz.

The Frequency Response Function (FRF) denoted $p(M_2)/i_s$ measured between the source loudspeaker current $i_s(t)$ and the acoustic pressure, $p(M_2, t)$, at M_2 with the blocked EA-NES inside the room is plotted Figure 7(b). The FRF was measured using a white noise in the frequency range $[30, 80]$ Hz as

target signal $e(t)$. Blocked EA-NES means that the front face membrane is covered by a rigid plate and does not interact with the acoustic pressure. This configuration defines the primary system as introduced Section 2. The first resonance frequency appears at $f \approx 43.8$ Hz corresponding to the $(1, 0, 0)$-mode and it is associated to a quality factor near to $Q_{100} \approx 133$. Note that these numerical values have been used in the previous theoretical analysis.

(a)

(b)

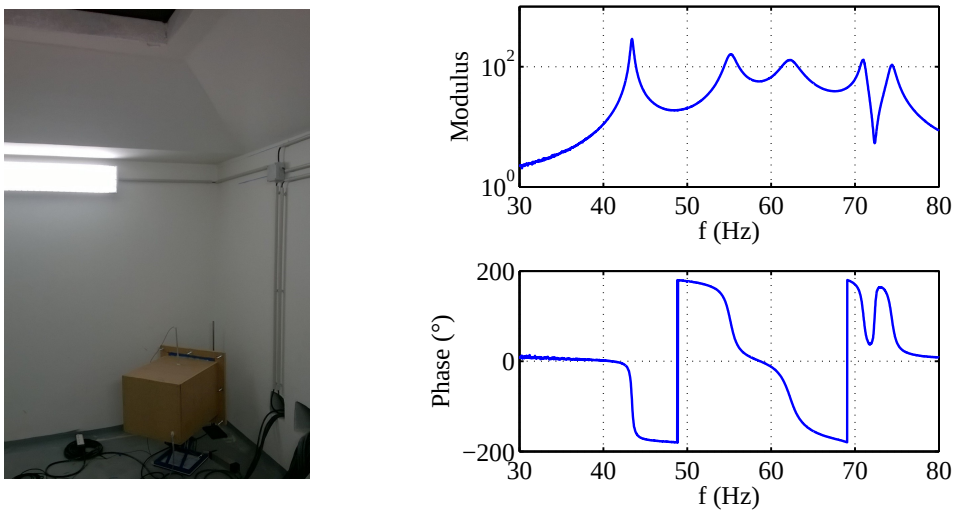

Figure 7: (a) Picture of the room with the EA-NES. (b) Frequency response function $p(M_2)/i_s$ measured with the blocked EA-NES inside the room.

4.1.1. The EA-NES

The tension of the membrane of the EA-NES must be tuned so that the resulting resonance frequency may be under the frequency of the targeted mode (43.8 Hz). The resonance at low level of the EA-NES is identified by using a short Kundt tube following the methodology described in [26]. This

measurement is made for some values of K for current and voltage feedback controls. Successive modifications of the pre-stress applied to the membrane were performed up to obtain the results displayed Table 1. For both current and voltage feedback controls, the resonance frequency is for $K = 0$ near the resonance frequency of the $(1, 0, 0)$-mode and decreases when the gain K increases.

Current	K	0	2.5	5.	7.5	15.
	f (Hz)	43.7	41	39.2	35.7	33.7
Voltage	K	0	100.	200.	400.	550.
	f (Hz)	43.9	31.1	27.7	24.6	24.

Table 1: Measured resonance frequency of the EA-NES versus gain K for current and voltage feedback controls

.

4.2. Nonlinear analysis

We measure the response of the cavity around its $(1, 0, 0)$-mode under sinusoidal forcing defined from a target signal

$$e(t) = E \sin(2\pi f_e + \phi_e) \tag{55}$$

which provides an input current signal to the source loudspeaker. Several measurements were performed increasing the forcing amplitude E from 0.01 to 0.25 and varying the forcing frequency from 42.5 Hz to 45 Hz, with a step of 0.1 Hz. The phase ϕ_e is introduced arbitrarily by the signal generator.

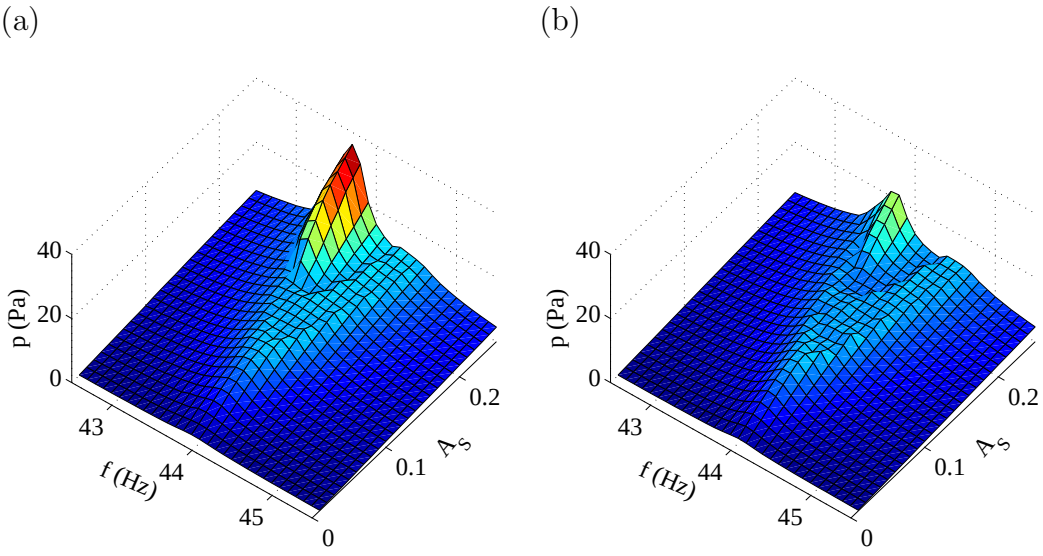

Figure 8: System with the EA-NES driven by current with $K = 7.5$: RMS values of the steady state regime of the acoustic pressure at the point M_3 as a surface level according to frequency and excitation amplitude: (a) measured values, (b) simulated values.

4.2.1. EA-NES driven in current with $K = 7.5$

We first consider the EA-NES with current feedback control and the gain value $K = 7.5$. TET has been observed with this configuration in the numerical simulation. The RMS values of the acoustic pressure measured at location M_3 are plotted in Fig. 8(a) as a surface level depending on the excitation frequency and the RMS values of the source loudspeaker current. The related numerical simulation are plotted Fig. 8(b). We can observe that the two surfaces are very similar. As expected a resonance peak around $f \approx 44$ Hz is observed on the acoustic pressure response at low excitation level. The flat surface at low excitation level becomes, due to the nonlinear behavior of the EA-NES, substantially disturbed by an increase in the excitation level accompanied by a reduction of the response level and the

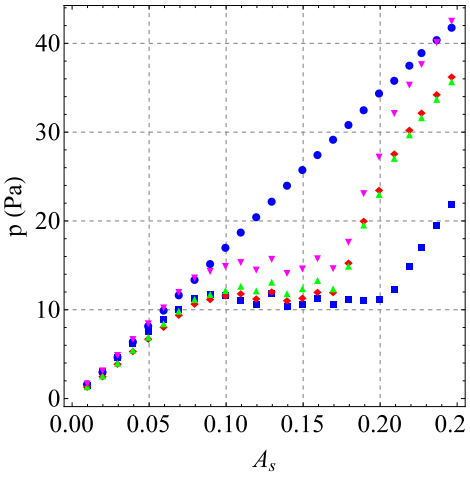

Figure 9: System with the EA-NES driven by current with $K = 7.5$: Ridge line of the RMS values of pressure measured at point M_1 (magenta triangle markers), at point M_2 (green triangle markers) and at point M_3 (red diamond markers), and simulated at point M_3 (blue square markers). The blue circle markers correspond to the ridge line at point M_3 with the blocked EA-NES.

occurrence, at high excitation level, of a resonance peak around $f \approx 43.6$ Hz, smaller than the resonance frequency observed at low excitation level. These behaviors were already reported in NES analysis [19, 18] and attributed to TET from the primary system to the NES. In order to quantify the triggering threshold and the width of the TET, ridge lines are extracted from each 3D plot of the acoustic pressure. The ridge line is defined as the maxima of the RMS values of the acoustic pressure for the considered frequency range for a given excitation amplitude. The measured ridge line at position M_3 (obtained from Fig. 8(a)) is displayed with the related simulations (obtained from Fig. 8(b)) in Fig. 9. Also plotted are the measured ridge line at positions M_1 and M_2. Furthermore we also present as a reference the

ridge line measured at position M_3 with the blocked EA-NES. In the blocked EA-NES configuration, the EA-NES is isolated from the acoustic field and cannot perform TET. It allows to measure the attenuation provided by the EA-NES as a function of the level of excitation. One can observe a limitation of the pressure (around 11 Pa) at positions M_1, M_2 and M_3 from $A_s = 0.08$ to $A_s = 0.17$. According to the reference ridge line, the EA-NES provides until 8 dB of attenuation in the pumping range. The power spent into the loudspeaker (around 2 W[25]) is in the range of the acoustic power absorbed from the room[27]. It is interesting because these orders of magnitude are consistent with self-powering by acoustic energy harvesting. This result is close to the numerical simulations except for the upper boundary of the excitation range which is overestimated. In this range the SMR regimes that mark the transfer of energy from the cavity to the EA-NES occur as it can be seen in Fig. 10 where three families of response regimes are illustrated depending of the excitation level. At low excitation level ($A_s = 0.03$), the regime is sinusoidal, the EA-NES do not act (Fig. 10(a,b)). For $A_s = 0.12$ (in the limitation range), a SMR regime occurs (Fig. 10(c,d)) and, for large excitation level ($A_s = 0.19$), the regime is again periodic (Fig. 10(e,f)). Note that we have chosen to plot the complete measured time responses including a first step with no source signal, a second step with source signal and a last step with no source signal. Furthermore one notices a good match between numerical simulation and measurements.

4.2.2. Influence of K in current and voltage modes

The influence of the parameters characterizing the active part of the EA-NES on the TET efficiency are investigated in order to validate the asymp-

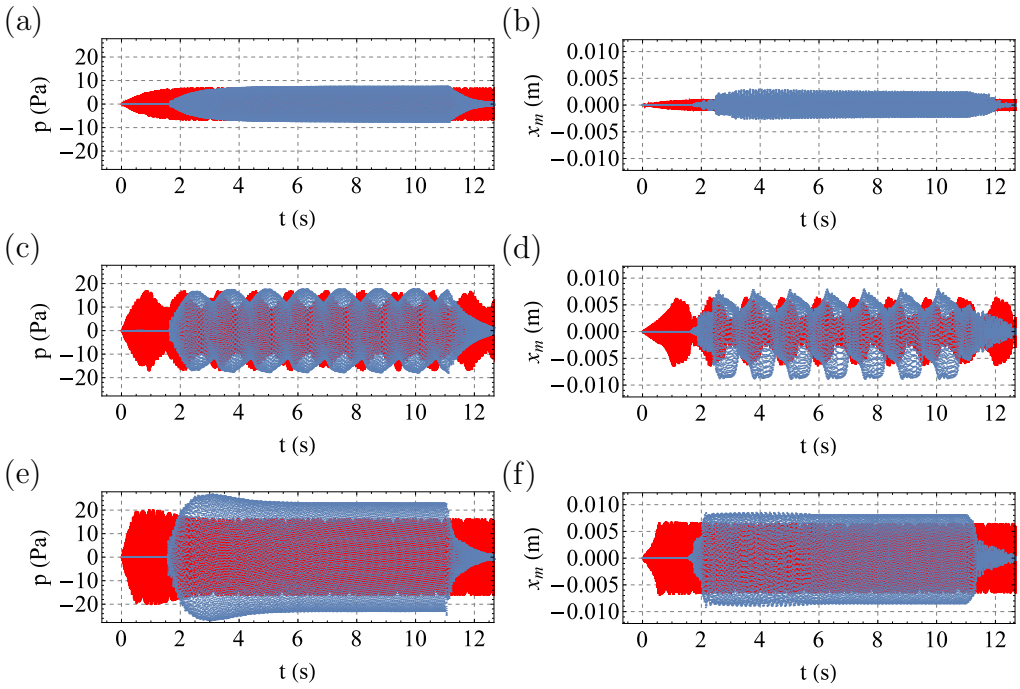

Figure 10: System with EA-NES driven by current with $K = 7.5$: (a, c, e) acoustic pressure at point M_3 and (b, d, f) displacement at the center of the membrane for $f_s = 43.9$ Hz and (a,b) $A_s = 0.03$, (c,d) $A_s = 0.12$ and (e,f) $A_s = 0.19$. Numerical results from Eq. (20-22) (red curves) and data (blue curves).

totic analysis discussed in Section 3. The parameters are: the feedback control mode of the loudspeaker (current versus voltage) and the gain K. The gain K varies from $K = 0$ to $K = 15$. when current feedback control is considered and $K = 550$. when voltage feedback control is considered. In all cases, the stability of the feedback control system is satisfied. For both feedback control modes, the value $K = 0$ is set with a shortcut on the input of the amplifier of the control loudspeaker and a gain set to the maximum.

We focus on the analysis to the ridge line (as defined in the previous section) of the acoustic pressure at position M_3. Indeed the ridge lines are

convenient to compare the triggering threshold and width of pumping regimes between the different configurations.

According to the Fig. 11(a), the triggering threshold of the TET depends on the gain K in the case of the current control as observed in the SIM in Fig. 4. Indeed, starting from $K = 2.5$, the triggering threshold increases from 9 Pa to 15 Pa. The same phenomenon is observed with the voltage drive but in a less pronounced way (see Fig. 11(b)). As shown in [18], the effect of the gain K is to decrease the resonance frequency of the EA-NES at low level. As a consequence the needed level of excitation to synchronize the EA-NES with the $(1, 0, 0)$-mode is increasing and one can observe in the related SIM that the fold points also increase. One can also observe that the excitation range where occurs the limitation of the pressure depends very little on the gain K.

At last the influence of the electrical drive of the EA-NES is investigated thanks to the comparison of the ridge lines obtained with each type of control. We only take account of the ridge lines where a limitation of pressure can be observed. Indeed these ridge lines correspond to the values of K for which the TET has been observed. In each case, we plot the lower and the higher ridge line obtained with one type of control. Theses pairs of curves are plotted in Fig. 11(c) with the reference ridge line obtained with the blocked EA-NES. It appears that the current control gives the ridge lines with the lowest triggering thresholds in comparison with the voltage control. We obtain 15 Pa for the highest triggering threshold with current whereas the lowest triggering threshold occurs at 25 Pa. From another hand the voltage control results in a largest range for the limitation of the pressure than current control (0.13

versus 0.09 for A_s).

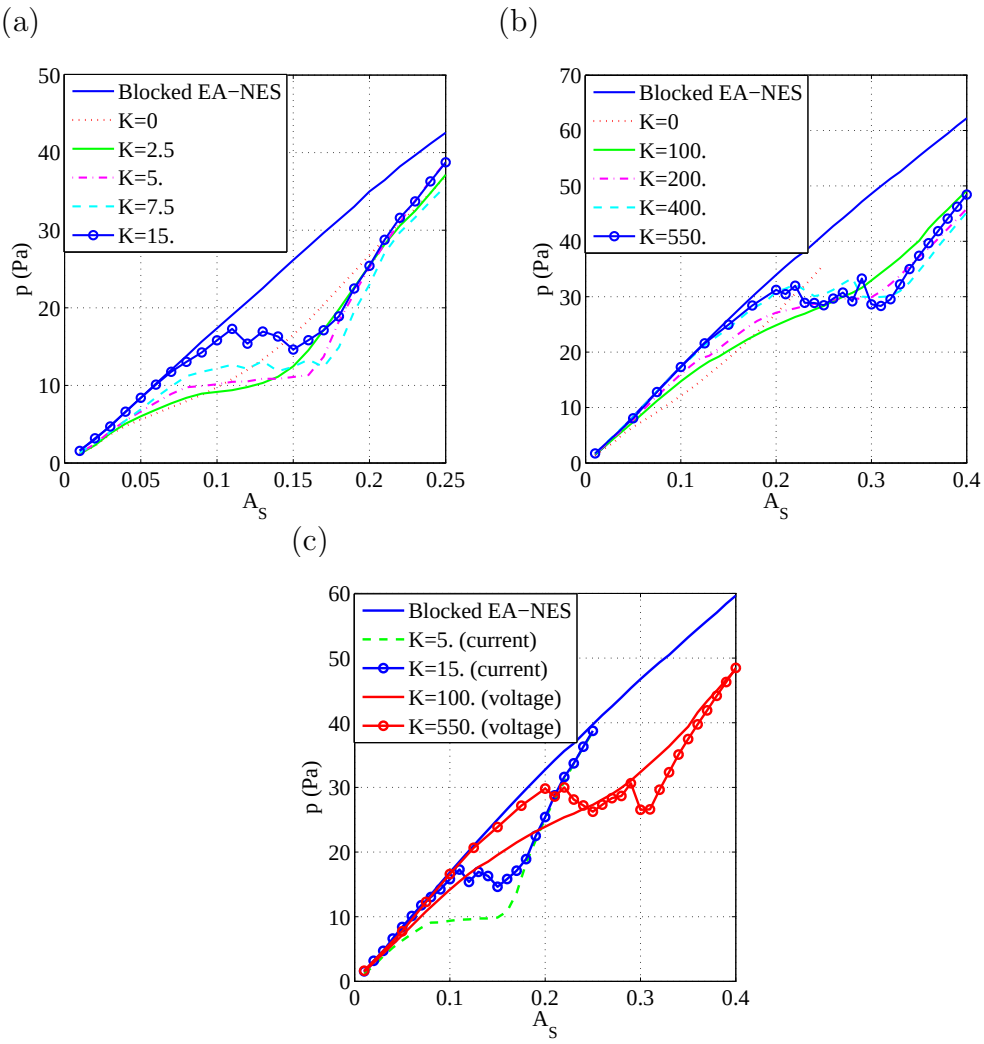

Figure 11: Ridge line of the RMS values of pressure measured at point M_3 for the system with EA-NES driven by (a) current, (b) voltage. (c) Comparison between current and voltage modes. In all plots, the blocked EA-NES is also reported.

5. Conclusion

We have studied a hybrid EA-NES coupled to a resonant room. We have modeled the electro-mechanical dynamics of the system. The asymptotic study of the model shows the existence of a critical value above which SMRs can exist. This threshold rises along with the gain of the control loop and is affected by the kind of control loop command law (voltage or current command law).

The experimental study shows that a hybrid EA-NES can work in a concrete building. It is able to limit the sound level in the room in its working range up to 8 dB for a footprint of only 0.2% of the room volume. The different regimes observed correspond well to previous observations for NESs, including SMRs, although the system or experimental conditions in previous works were far from this study's ones. Unlike previous acoustical studies, here the SMR responses are simulated with a good quantitative agreement, in voltage or current command law. We have also simulated and observed that the thresholds defining the working range of the NES can be tuned electrically by setting the gain K of the control loop. The thresholds are at sound levels much lower than in the previous studies [18] where the primary system and its coupling to the EA-NES were different.

This work opens the way to direct applications for acoustic noise treatment. It permits to envision further studies in several directions, like developments of the control law (adaptive tuning) in view of particularly reducing the the triggering threshold of the TET, or the merging of the EA-NES membrane and loudspeaker into one part only.

6. Acknowledgments

The first author acknowledges DGA-France for the financial support.

The authors thank P. Herzog [7] for his enriching inputs.

This work was done in the framework of the Labex MEC.

Appendix A. Fixed points and folded singularities of the slow-flow

This appendix characterizes the fixed points and folded singularities of the slow-flow from the slow subsystem Eqs. (41) to (43).

Substituting Eqs. (45) and (46) into Eqs. (41), the slow subsystem can be written only with respect to the variable ϕ_2 as

$$\begin{aligned}(\phi_2 F(|\phi_2|))' &= f_1(\phi_2 F(|\phi_2|), \phi_2, \frac{\bar{k}_{21}}{\gamma_{\rm LS} - \bar{k}_{22} - j\lambda_{\rm LS}}\phi_2), \\ &= j\frac{\beta}{2} + f_{1\phi_2}(|\phi_2|) \end{aligned} \tag{A.1}$$

where

$$\begin{aligned} f_{1\phi_2}(x) &= \frac{j}{8}\left((4j\lambda_{\rm p} - 8\bar{\sigma} + 4\mu_{\rm m}\mu_{\rm p})F(|\phi_2|) + (3\bar{k}_{3\rm m}\mu_{\rm p} + j\lambda_{2\rm m}\mu_{\rm p})|\phi_2|^2\right)\phi_2 \\ &\quad + \frac{j}{8}\left(4\mu_{\rm p}(j\lambda_{\rm m} + \bar{k}_{11}) + \frac{4\bar{k}_{12}\mu_{\rm p}\bar{k}_{21}}{\gamma_{\rm LS} - \bar{k}_{22} - j\lambda_{\rm LS}}\right)\phi_2. \end{aligned} \tag{A.2}$$

Using the polar coordinates (49) for $i = 2$ with now N_2 and θ_2 being τ dependent, and separating real and imaginary parts, Eq. (A.1) takes (after some calculation steps) the following form

$$a_{11}(N_2)N_2' + a_{12}(N_2)\theta_2' = b_1(N_2, \theta_2), \tag{A.3}$$

$$a_{21}(N_2)N_2' + a_{22}(N_2)\theta_2 = b_2(N_2, \theta_2) \tag{A.4}$$

with

$$a_{11}(x) = xF'_R(x) + F_R(x), \qquad a_{12}(x) = -rF_I(x), \tag{A.5}$$

$$a_{21}(x) = xF'_I(x) + F_I(x), \qquad a_{22}(x) = xF_R(x), \tag{A.6}$$

$$b_1(x,\theta) = \Re(f_{1\phi_2}(x)) + \frac{\beta}{2}\sin(\theta), \qquad b_2(x,\theta) = \Im(f_{1\phi_2}(x)) + \frac{\beta}{2}\cos(\theta) \tag{A.7}$$

where $\Re(.)$ (respectively $\Im(.)$) denotes the real part (respectively imaginary part) of (.)

Systems of Eqs. (A.3) and (A.4) can be finally reduced (after some calculation steps) to the following form

$$g(N_2)N'_2 = f_{N_2}(N_2,\theta_2), \tag{A.8}$$

$$g(N_2)\theta'_2 = f_{\theta_2}(N_2,\theta_2) \tag{A.9}$$

where

$$g(x) = a_{11}(x)a_{22}(x) - a_{12}(x)a_{21}(x) = H'(x)/2, \tag{A.10}$$

$$f_{N_2}(x,\theta) = a_{22}(x)b_1(x,\theta) - a_{12}(x)b_2(x,\theta), \tag{A.11}$$

$$f_{\theta_2}(x,\theta) = -a_{21}(x)b_1(x,\theta) + a_{11}(x)b_2(x,\theta). \tag{A.12}$$

From Eqs. (A.8) and (A.9) it is possible to detect fixed points and folded singularities.

The (regular) fixed points of Eqs. (A.8) and (A.9), denoted hereafter (N_2^e, θ_2^e), are defined by

$$f_{N_2}(N_2^e,\theta_2^e) = 0,\ f_{\theta_2}(N_2^e,\theta_2^e) = 0 \text{ with } g(N_2^e) \neq 0. \tag{A.13}$$

For $\epsilon << 1$, the (regular) fixed points are good approximation of the fixed points of the full system Eqs. (29) to (31) corresponding to a periodic solution

of the adimensional model. The stability of the periodic solution is found by looking at the sign of the real parts of the eigenvalues of the Jacobian matrix of differential system Eqs. (A.8) and (A.9).

The folded singularities of Eqs. (A.8) and (A.9), denoted hereafter (N_2^s, θ_2^s), are defined by

$$f_{N_2}(N_2^s, \theta_2^s) = 0,\ f_{\theta_2}(N_2^s, \theta_2^s) = 0 \text{ and } g(N_2^s) = 0. \tag{A.14}$$

A folded singularity is a fold point ($N_2^s = N_2^{f1}$ or N_2^{f2}) satisfying

$$f_{N_2}(N_2^{f1/2}, \theta_2^s) = 0,\ f_{\theta_2}(N_2^{f1/2}, \theta_2^s) = 0 \tag{A.15}$$

where $N_2^{f1/2}$ denotes N_2^{f1} or N_2^{f2}.

Recalling Eqs. (A.7), (A.11) and (A.12), Eq. (A.15) is reduced to the linear system with respect to $(\sin(\theta_2^s), \cos(\theta_2^s))$ as

$$\frac{\beta}{2}(a_{22}(N_2^{f1/2})\sin(\theta_2^s) - a_{12}(N_2^{f1/2})\cos(\theta_2^s)) = d_1(N_2^{f1/2}), \tag{A.16}$$

$$\frac{\beta}{2}(-a_{21}(N_2^{f1/2})\sin(\theta_2^s) + a_{11}(N_2^{f1/2})\cos(\theta_2^s)) = d_2(N_2^{f1/2}) \tag{A.17}$$

where the functions $d_1(x)$ and $d_2(x)$ are not explicitly given.

The associated determinant of this linear system is equal to zero showing that one of the two equations can be removed. Therefore, the folded singularities can be only defined by Eq. (A.17) as

$$-a_{21}(N_2^{f1/2})\sin(\theta_2^s) + a_{11}(N_2^{f1/2})\cos(\theta_2^s) = \frac{2}{\beta}d_2(N_2^{f1/2}) \tag{A.18}$$

which can be solved with respect to θ_2^s giving the following pair of solutions

(for each fold point)

$$\theta_2^{s1/2} = \arcsin \frac{-a_{21}(N_2^{f1/2})}{\sqrt{a_{11}(N_2^{f1/2})^2 + a_{12}(N_2^{f1/2})^2}} \tag{A.19}$$

$$\pm \arccos \frac{2d_2(N_2^{f1/2})}{\beta\sqrt{a_{11}(N_2^{f1/2})^2 + a_{12}(N_2^{f1/2})^2}} \tag{A.20}$$

if the condition

$$|\frac{2d_2(N_2^{f1/2})}{\beta\sqrt{a_{11}(N_2^{f1/2})^2 + a_{12}(N_2^{f1/2})^2}}| \leq 1 \tag{A.21}$$

is satisfied.

Condition Eq. (A.21) shows that the fold point $N_2^{f1/2}$ is a folded singularity for values of excitation level β such that

$$\beta_{\mathrm{cr}1/2} = |\frac{2d_2(N_2^{f1/2})}{\sqrt{a_{11}(N_2^{f1/2})^2 + a_{12}(N_2^{f1/2})^2}}| < \beta. \tag{A.22}$$

However, Condition (A.22) is necessary but not sufficient to guarantee the stability of SMR regimes. Under certain conditions, the slow flow may be attracted to another stable response. This mechanism of annihilation of SMR is explained in detail in [21] and to access this possibility, a procedure of $1D$ mapping has been also developed. We have not extended this procedure to our case.

References

References

[1] G. Yu, L. Cheng, Location optimization of a long t-shaped acoustic resonator array in noise control of enclosures, Journal ofSoundandVibration 328 (2009) 4256.

[2] T. Cambonie, F. Mbailassem, E. Gourdon, Bending a quarter wavelength resonator : Curvature effects on sound absorption properties, Applied Acoustics 131 (2018) 87–102.

[3] H. Lissek, R. Boulandet, R. Fleury, Electroacoustic absorbers: Bridging the gap between shunt loudspeakers and active sound absorption, J. Acoust. Soc. Am 129 (2011) 2968–2978.

[4] R. Boulandet, H. Lissek, Toward broad band electroacoustic resonators through optimized feedback control strategies, Journal of Sound and Vibration 333 (2014) 4810–4825.

[5] O. Lacour, M. Galland, D. Thenail, Preliminary experiments on noise reduction in cavities using active impedance changes, Journal of Sound and Vibration 230 (1) (2000) 69–99.

[6] J. Dupont, M. Galland, Active absorption to reduce the noise transmitted out of an enclosure, Applied Acoustics 70 (2009) 142–152.

[7] M. Melon, P. Herzog, A. Sitel, M. Galland, One dimensional study of a module for active/passive control of both absorption and transmission, Applied Acoustics 73 (2012) 234–242.

[8] A. Vakakis, O. Gendelman, L. Bergman, D. McFarland, G. Kerschen, Y. Lee, Nonlinear targeted energy transfer in mechanical and structural systems, Vol. 156 of Solid mechanics and its applications, Springer, 2008.

[9] E. Gourdon, N. Alexander, C. Taylor, C.-H. Lamarque, S. Pernot, Nonlinear energy pumping under transient forcing with strongly nonlinear

coupling: Theoretical and experimental results, Journal of Sound and Vibration 300 (2007) 522–551.

[10] G. Sigalov, O. Gendelman, M. AL-Shudeifat, L. Manevitch, A. Vakakis, L. Bergman, Resonance captures and targeted energy transfers in an inertially-coupled rotational nonlinear energy sink, Nonlinear Dyn 69 (2012) 1693–1704.

[11] E. Gourc, S. Seguy, G. Michon, A. Berlioz, B. Manne, Quenching chatter instability in turning process with a vibro-impact nonlinear energy sink, Journal of Sound and Vibration 355 (2015) 392–406.

[12] P.-O. Mattei, R. Ponçot, M. Pachebat, R. Côte, Nonlinear targeted energy transfer of two coupled cantilever beams coupled to a bistable light attachment, Journal of Sound and Vibration 373 (Supplement C) (2016) 29–51. doi:https://doi.org/10.1016/j.jsv.2016.03.008. URL http://www.sciencedirect.com/science/article/pii/S0022460X16002376

[13] E. Gourdon, A. T. Savadkoohi, V. Alamo Varga, Targeted energy transfer from one acoustical mode to an helmholtz resonator with nonlinear behavior, Journal of Vibration and Acoustic 140 (2018) 061005–1–061005–8.

[14] B. Cochelin, P. Herzog, P.-O. Mattei, Experimental evidence of energy pumping in acoustics, C. R. Mécanique 334 (11) (2006) 639–644.

[15] R. Bellet, B. Cochelin, P. Herzog, P.-O. Mattei, Experimental study of targeted energy transfer from an acoustic system to a nonlinear membrane absorber, Journal of Sound and Vibration 329 (2010) 2768–2791.

[16] J. Shao, B. Cochelin, Theoretical and numerical study of targeted energy transfer inside an acoustic cavity by a non-linear membrane absorber, International Journal of Non-Linear Mechanics 64 (2014) 85–92.

[17] R. Mariani, S. Bellizzi, B. Cochelin, P. Herzog, P.-O. Mattei, Toward an adjustable nonlinear low frequency acoustic absorber, Journal of Sound and Vibration 330 (2011) 5245–5258.

[18] P.-Y. Bryk, S. Bellizzi, R. Côte, Experimental study of a hybrid electro-acoustic nonlinear membrane absorber, Journal of Sound and Vibration 424 (2018) 224–237.

[19] R. Bellet, B. Cochelin, R. Côte, P.-O. Mattei, Enhancing the dynamic range of targeted energy transfer in acoustics using several nonlinear membrane absorbers, Journal of Sound and Vibration 331 (26) (2012) 5657–5668.

[20] R. Côte, M. Pachebat, S. Bellizzi, Experimental evidence of simultaneous multi-resonance noise reduction using an absorber with essential nonlinearity under two excitation frequencies, Journal of sound and vibration 333 (2014) 5057–5076.

[21] Y. Starosvetsky, O. Gendelman, Strongly modulated response in forced 2DOF oscillatory system with essential mass and potential asymmetry, Physica D 237 (2008) 1719–1733.

[22] L. Manevitch, Complex representation of dynamics of coupled nonlinear oscillators, in: L. Uvarova, A. Arinstein, A. Latyshev (Eds.), Mathematical Models of Non-Linear Excitations, Transfer, Dynamics, and Control

in Condensed Systems and Other Media, Springer US, 1999, pp. 269–300.

[23] N. Fenichel, Geometric singular perturbation theory for ordinary differential equations, J. Differ. Equ 98 (1979) 53–98.

[24] M. Desroches, J. Guckenheimer, B. Krauskopf, C. Kuehn, H. M. Osinga, M. Wechselberger, Mixed-mode oscillations with multiple time scales, SIAM Review 54, (2) (2012) 211–288.

[25] P.-Y. Bryk, Pompage énergétique en acoustique par absorbeur dynamique non-linéaire hybride passif-actif, Ph.D. thesis, AIX-MARSEILLE UNIVERSITÉ - ED 353 Sciences pour l'ingénieur : Mécanique, Physique, Micro et Nanoélectronique (2018).

[26] A. Chauvin, M. Monteil, S. Bellizzi, R. C P. Herzog, M. Pachebat, Acoustic characterization of a nonlinear vibroacoustic absorber at low frequencies and high sound levels, Journal of Sound and Vibration 416 (2018) 244–257.

[27] S. Bellizzi, R. Côte, M. Pachebat, Responses of a two degree-of-freedom system coupled to a nonlinear damper under multi-forcing frequencies, Journal of Sound and Vibration 332 (2013) 1639–1653.